REVIEW SUMMARY

APPLIED OPTICS

Optically resonant dielectric nanostructures

Arseniy I. Kuznetsov, Andrey E. Miroshnichenko, Mark L. Brongersma,* Yuri S. Kivshar,* Boris Luk'yanchuk*

BACKGROUND: Nanoscale optics is usually associated with plasmonic structures made of metals such as gold or silver. However, plasmonics suffers from high losses of metals, heating, and incompatibility with complementary metal oxide semiconductor fabrication processes. Recent developments in nanoscale optical physics have led to a new branch of nanophotonics aiming at the manipulation of optically induced Mie resonances in dielectric and semiconductor nanoparticles with high refractive indices. Such particles offer unique opportunities for reduced dissipative losses and large resonant enhancement of both electric and magnetic near-fields. Semiconductor nanostructures also offer longer excited-carrier lifetimes and can be electrically doped and gated to realize subwavelength active devices. These recent developments revolve closely around the nature of the optical resonances of the structures and how they can be manipulated in individual entities and in complex particle arrangements such as metasurfaces. Resonant high-index dielectric nanostructures form new building blocks to realize unique functionalities and novel photonic devices.

ADVANCES: We discuss the key advantages of resonant high-index nanostructures, associated new physical effects, and applications for nanoantennas, optical sensors, nonlinear devices, and flat optics. For a subwavelength high-index dielectric particle illuminated by a plane wave, electric and magnetic dipole resonances have comparable strengths. The resonant magnetic response results from a coupling of incoming light to the circular displacement currents of the electric field, when the wavelength inside the particle becomes comparable to its diameter $d = 2R \approx \lambda/n$, where R is the nanoparticle radius, n is its refractive index, and λ is the wavelength of light. At the wavelength of a magnetic resonance, the excited magnetic dipole mode of a high-index dielectric sphere may provide a dominant contribution to the scattering efficiency exceeding the contribution of other multipoles by orders of magnitude.

Nanophotonic structures composed of dielectric resonators can exhibit many of the same features as plasmonic nanostructures, including enhanced scattering, high-frequency magnetism, and negative refractive index. The specific design and parameter engineering of all-dielectric nanoantennas and metasurfaces give rise to superior performance in comparison to their lossy plasmonic counterparts. Spectral signatures of the Mie-type resonances of these structures are revealed by using far-field spectroscopy while tuning geometrically their resonance properties. A special case is realized when the electric and magnetic resonances spectrally overlap; the impedance matching eliminates the backward scattering, leading to unidirectional scattering and Huygens metasurfaces. A variety of nanoparticle structures have been studied, including dielectric oligomers as well as metasurfaces and metadevices. The magnetic resonances lead to enhanced nonlinear response, Raman scattering, a novel Brewster effect, sharp Fano resonances, and highly efficient sensing and photodetection.

ON OUR WEBSITE

Read the full article at http://dx.doi.org/10.1126/science.aag2472

OUTLOOK: The study of resonant dielectric nanostructures has been established as a new research direction in modern nanophotonics. Because of their unique optically induced electric and magnetic resonances, high-index nanophotonic structures are expected to complement or even replace different plasmonic components in a range of potential applications. The unique low-loss resonant behavior allows reproduction of many subwavelength resonant effects demonstrated in nanophotonics without much energy dissipation into heat. In addition, the coexistence of strong electric and magnetic resonances, their interference, and resonant enhancement of the magnetic field in dielectric nanoparticles bring entirely novel functionalities to simple geometries largely unexplored in plasmonic structures, especially in the nonlinear regime or in optoelectronic device applications. ■

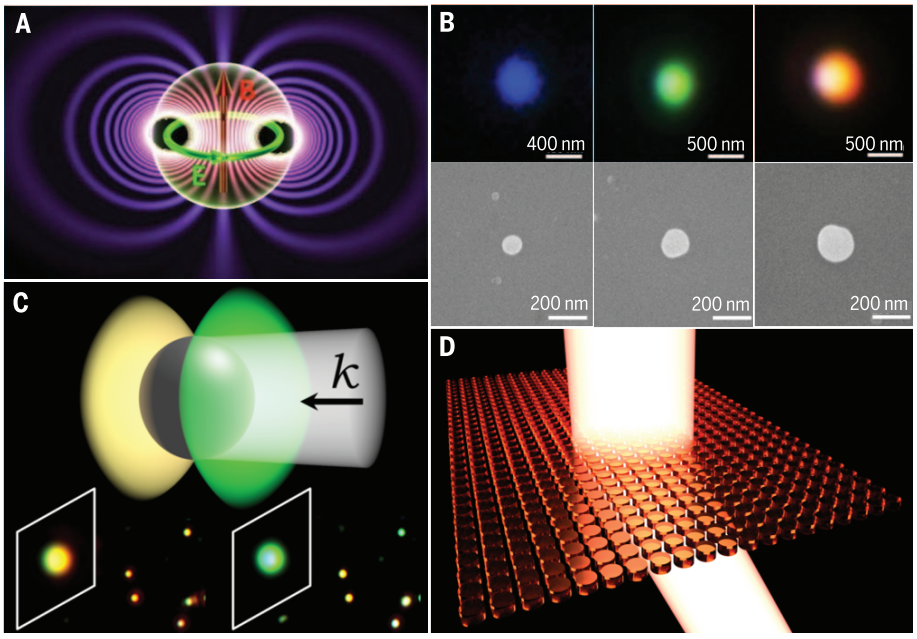

Manifestations of all-dielectric resonant nanophotonics. (**A**) Structure of the fields near the magnetic dipole resonance. (**B**) Experimental demonstration of optical magnetic response shown through optical dark-field and scanning electron microscope images (top and bottom, respectively). (**C**) Unidirectional light scattering by a single dielectric nanoparticle for overlapping electric and magnetic dipole resonances, where **k** is the wave vector of the incident white light. (**D**) Light manipulation with highly transparent Huygens metasurfaces.

The list of author affiliations is available in the full article online.
*Corresponding author. Email: ysk@internode.on.net (Y.S.K.); boris_l@dsi.a-star.edu.sg (B.L.); brongersma@stanford.edu (M.L.B.)
Cite this article as A. I. Kuznetsov *et al.*, *Science* **354**, aag2472 (2016). DOI: 10.1126/science.aag2472

Downloaded from https://www.science.org at Moscow State University on March 10, 2022

REVIEW

APPLIED OPTICS

Optically resonant dielectric nanostructures

Arseniy I. Kuznetsov,[1] Andrey E. Miroshnichenko,[2] Mark L. Brongersma,[3]* Yuri S. Kivshar,[2]* Boris Luk'yanchuk[1,4]*

Rapid progress in nanophotonics is driven by the ability of optically resonant nanostructures to enhance near-field effects controlling far-field scattering through intermodal interference. A majority of such effects are usually associated with plasmonic nanostructures. Recently, a new branch of nanophotonics has emerged that seeks to manipulate the strong, optically induced electric and magnetic Mie resonances in dielectric nanoparticles with high refractive index. In the design of optical nanoantennas and metasurfaces, dielectric nanoparticles offer the opportunity for reducing dissipative losses and achieving large resonant enhancement of both electric and magnetic fields. We review this rapidly developing field and demonstrate that the magnetic response of dielectric nanostructures can lead to novel physical effects and applications.

Ever since Lord Rayleigh clarified why our sky is blue, the study of light scattering by nanoparticles has been an important part of optical science. Later, Gustav Mie explained a variation in colors of colloidal solutions of gold nanoparticles in terms of their size distribution, thereby opening up the possibility of using resonant nanoscale scatterers to control an optical response. Recent decades have witnessed a growing interest in the study of plasmonic nanoparticles made of gold or silver (*1*). The resonant optical modes supported by such structures endow them with an ability to manipulate light at the nanoscale. This notion has stimulated the development of a diverse set of applications including biosensors, thermotherapy, solar cells, and information storage. However, up to now only a small fraction of plasmonics applications have been realized in practice, mainly due to high losses of metals at visible frequencies and their incompatibility with complementary metal oxide semiconductor (CMOS) fabrication processes. Whereas new materials with improved plasmonic properties have been proposed (*2*), there has been a growing understanding that the optical resonances of high-index dielectric and semiconductor nanostructures can also facilitate light manipulation below the free-space diffraction limit. These structures offer very low optical losses, a wealth of distinct optical resonances, and an opportunity to manipulate the resonances by electrical doping and gating of the mobile carrier density. Many dielectrics and semiconductors are also materials that are compatible with semiconductor device technologies.

For these reasons, it is of great value to analyze how such high-index dielectric structures can be used as building blocks with unique optical functionalities for real metadevices and novel structures. It remains to be determined where exactly they can add much value to their metallic counterparts. Studies currently in progress derive inspiration from century-old studies on light scattering while also advancing our knowledge of photonic crystals and metamaterials. Logically, these studies revolve closely around the nature of the optical resonances of the nanostructures and how they can be manipulated in individual entities as well as complex particle arrangements. We review the basic optical properties of nanostructures composed of resonant high-index nanoparticles, analyze recent advances in this area, and provide a perspective that will help to direct future research.

Mie resonances in subwavelength particles

To illustrate the fundamental properties of light scattering by nanoparticles, we consider the case of a spherical particle illuminated by a plane wave, for which an exact analytical solution of Maxwell's equations exists. According to Mie theory (*3*), both metallic and dielectric spherical particles can possess strong scattering resonances (Fig. 1A). In the case of lossless and nonmagnetic materials, their scattering properties depend only on two parameters: the dielectric permittivity ε and a size parameter q that is proportional to the ratio between the nanoparticle radius R and the wavelength of light λ ($q = 2\pi R/\lambda$). For a fixed size parameter, the difference between metallic and dielectric particles is in the sign of the dielectric permittivity, which is negative for metals and positive for dielectrics. Small metallic spheres ($q < 1$) produce only localized surface plasmon resonances of an electric type—dipole, quadrupole, etc.—while their magnetic response remains almost negligible because of a vanishing field inside the sphere (Fig. 1A). To generate a magnetic response from metallic structures, the particle's geometry should be changed. For example, a split-ring resonator (*4*) works similarly to an effective LC circuit (i.e., inductor-capacitor circuit) with the enhancement of the magnetic field in the center. For dielectric particles, we can observe both electric- and magnetic-type responses of comparable strengths (Fig. 1A). The resonant magnetic dipole response results from a coupling of incoming light to the circular displacement currents of the electric field, owing to the field penetration and phase retardation inside the particle. This occurs when the wavelength inside the particle becomes comparable to the particle's diameter $2R \approx \lambda/n$ (Fig. 1B). The field structure of the four major resonant modes in high-index dielectric particles—magnetic dipole, electric dipole, magnetic quadrupole, and electric quadrupole—is shown in Fig. 1C. At the wavelength of a magnetic resonance, the excited magnetic dipole mode of a high-index dielectric sphere may provide a major contribution to the scattering efficiency, exceeding that of other multipoles by orders of magnitude.

From Mie theory, it follows that the maximum achievable scattering efficiency for a specific multipolar excitation of a subwavelength particle depends only on the resonance frequency and not the type of material (*5*). This suggests that many plasmonic effects observed for the scattering of light by metallic nanoparticles can be realized with high-index dielectric nanoparticles. Figure 1B shows the scaling of different resonances with respect to the refractive index n. For $n > 2$, all main multipoles are well defined, and their spectral positions correspond to a fixed ratio of the wavelength inside the particle, λ/n, to its diameter, $2R$. The scattering efficiency of all multipoles also increases with increasing n (*6*–*9*).

Strong, optically induced magnetic dipole resonances in high-index dielectric nanoparticles can be achieved not only for spheres but also for spheroids (*10*, *11*), disks and cylinders (*12*), rings (*13*), and many other geometries (*14*). This provides important opportunities for designing a variety of all-dielectric nanostructures with desirable spectral positions of the resonances. By changing the geometrical parameters of the particles, the spectral positions of both electric and magnetic dipole resonances can be tuned independently, interchanging or overlapping spectrally at a single frequency for simple geometries (*11*, *12*, *15*).

Observation of optical magnetic resonances in dielectric nanoparticles

Experimental observation of magnetic resonances in dielectric particles at optical frequencies

[1]Data Storage Institute, A*STAR (Agency for Science, Technology and Research), 138634 Singapore. [2]Nonlinear Physics Centre, Research School of Physics and Engineering, Australian National University, Canberra, ACT 2601, Australia. [3]Geballe Laboratory for Advanced Materials, Stanford University, Stanford CA 94305, USA. [4]Division of Physics and Applied Physics, School of Physical and Mathematical Sciences, Nanyang Technological University, 637371 Singapore.
*Corresponding author. Email: ysk@internode.on.net (Y.S.K.); boris_l@dsi.a-star.edu.sg (B.L.); brongersma@stanford.edu (M.L.B.)

Downloaded from https://www.science.org at Moscow State University on March 10, 2022

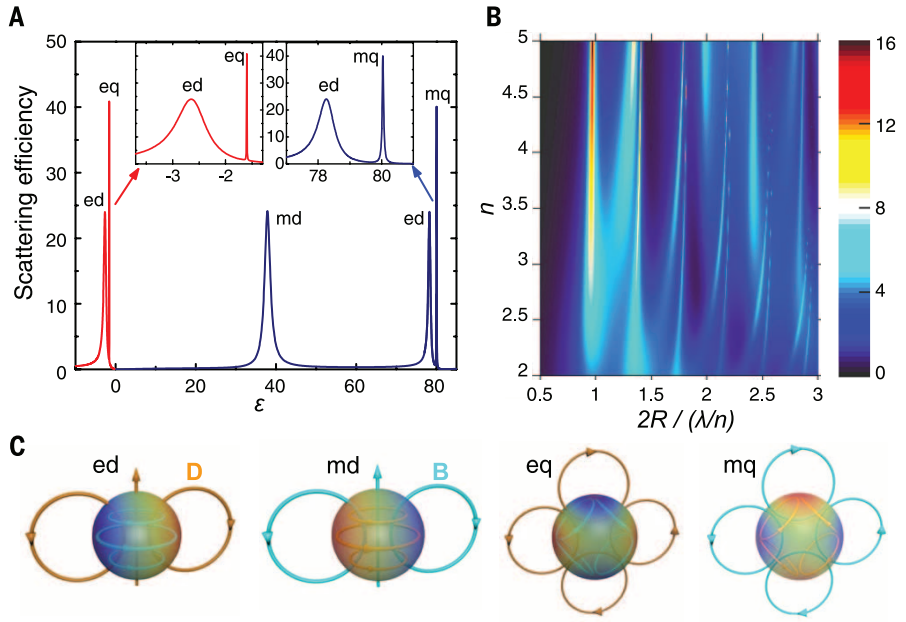

Fig. 1. Mie resonances of a spherical particle. (**A**) Scattering efficiency (dimensionless ratio of scattering cross section to geometrical cross section of the particle) versus dielectric permittivity ε (lossless particle, q = 0.5) for plasmonic (ε < 0) and dielectric (ε > 0) materials. Abbreviations for resonances: ed, electric dipole; eq, electric quadrupole; md, magnetic dipole; mq, magnetic quadrupole. Higher-order multipole modes are not shown for the sake of simplicity. (**B**) Scattering efficiency of a lossless dielectric particle (color scale at right) as a function of refractive index n and size parameter. (**C**) Illustration of electric and magnetic field structures for different electric and magnetic resonances supported by a spherical dielectric particle.

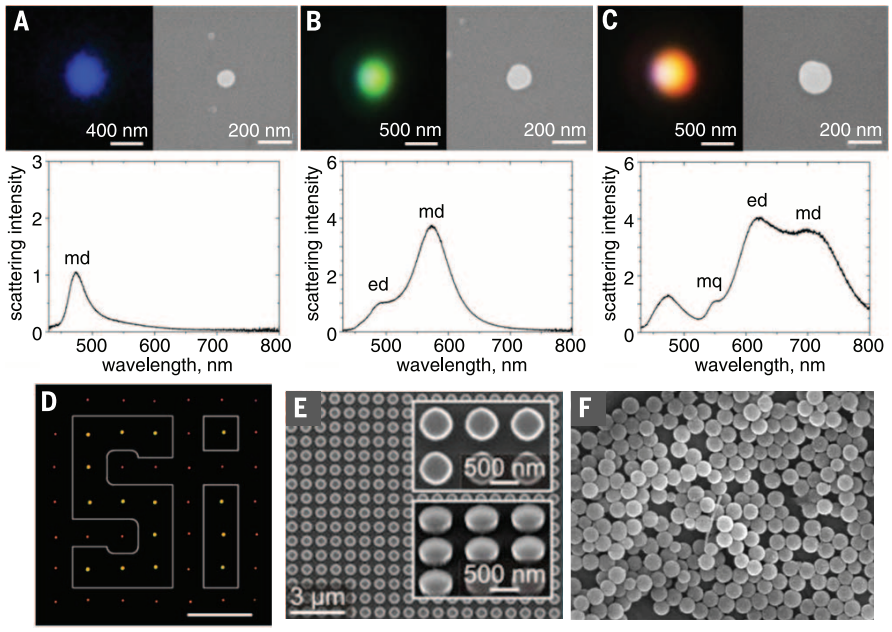

Fig. 2. Demonstration of optical magnetic response and examples of resonant silicon nanostructures. (**A** to **C**) Dark-field optical microscope images (top left), scanning electron microscope (SEM) images (top right), and dark-field scattering spectra (bottom) of spherical Si nanoparticles with approximate diameters of 100 nm (A), 140 nm (B), and 180 nm (C) (*8*). Abbreviations for resonances are as in Fig. 1. (**D**) Dark-field microscope image of laser-printed Si nanoparticle arrays. Si is crystallized inside the marked areas by additional laser irradiation, producing a change in color (*22*); scale bar, 10 μm. (**E**) Lithographically fabricated Si nanodisk arrays with varied spectral positions of the electric and magnetic resonances (*15*). (**F**) Monodispersed silicon nanoparticles resonant at near-IR frequencies prepared by chemical synthesis (*25*).

[mid-infrared (IR)] was reported for silicon carbide microrods (*16*). Later, dielectric and semiconductor microrods and nanorods were observed to exhibit scattering resonances in the visible and near-IR spectral range [see, e.g., (*17*–*19*)]. It was also pointed out (*6*, *7*) that silicon (Si) nanospheres with sizes ranging from 100 to 300 nm support strong magnetic and electric dipole resonances in the visible and near-IR spectral range. Although Si is not a completely loss-free material, its absorption in the visible spectrum is much lower than that of metals, making it a good material for the study of Mie resonances.

An experimental demonstration of electric and magnetic dipole resonances at visible wavelengths was first reported for spherical Si nanoparticles fabricated by femtosecond laser ablation on silicon and glass substrates (*8*, *20*). Different colors observed in dark-field microscope images (Fig. 2, A to C) correspond to magnetic dipole resonances of almost perfect spherical Si nanoparticles with sizes ranging from 100 to 200 nm (*8*). A recently developed laser-induced transfer method allows the generation of arrays of resonant nanoparticles with almost perfect spherical shape (Fig. 2D) (*21*, *22*). However, from the viewpoint of practical applications, conventional electron beam lithography and photolithography provide much better reproducibility and control over the structural parameters (Fig. 2E) (*15*, *17*). Soft-imprint lithography (*23*), nanosphere lithography (*24*), and chemical synthesis (Fig. 2F) (*25*) were also used for generating silicon nanostructures with the required parameters to display strong scattering resonances in the visible and near-IR spectrum. Apart from silicon, group IV and group III-V semiconductors with refractive indices above 2 might have similar optical properties depending on their absorption and refractive index in a specific wavelength range. For example, magnetic and electric dipole resonances were recently observed experimentally in gallium arsenide (GaAs) nanodisks in the visible spectrum (*26*) and tellurium (Te) cubes in the mid-IR spectrum (*27*).

Directional scattering of light

Any particle much smaller than the wavelength of light (R << λ) behaves as an electric dipole that scatters light symmetrically in the plane transverse to the dipole axis. To achieve an asymmetry in the light scattering, interference effects of a few or several different modes can be exploited. For plasmonic particles, the asymmetric scattering may be attributable to the Fano resonance resulting from interference of a broad electrical dipole and narrow quadrupole (or higher-order) modes (*28*, *29*). However, losses of typical plasmonic metals are too large and preclude a clear observation of this effect in a single spherical nanoparticle. In high-index dielectric nanospheres, strong directional scattering of light results from the interference of magnetic and electric dipole responses excited simultaneously in the nanoparticle with comparable strength. Using Mie theory for a spherical dielectric nanoparticle, it can be shown that when

Downloaded from https://www.science.org at Moscow State University on March 10, 2022

electric (a_1) and magnetic (b_1) dipole coefficients (*3*) coincide ($a_1 = b_1$) and other higher-order modes are negligible, the backward scattering vanishes (Fig. 3, A to C) (*11*, *30*, *31*). This is conceptually similar to the condition for the zero-backward scattering derived by Kerker *et al.* in 1983 (*32*) for a particle having similar electric and magnetic properties, $\varepsilon = \mu$, often called the first Kerker condition. Although the total suppression of the forward scattering is forbidden by the optical theorem (*33*), it is also possible to find the other condition for a minimal ratio of the forward and backward scattering, often called the second Kerker condition (*34*).

Experimental verification of the Kerker-type asymmetry in the scattering of electromagnetic waves by high-index dielectric particles was reported in the microwave regime (*35*) for spherical ceramic particles with diameter of 18 mm and refractive index of 4. Microwave experiments allowed direct measurements of angular scattering patterns (Fig. 3D). Asymmetric scattering by Si nanoparticles at visible frequencies was demonstrated shortly thereafter (Fig. 3E) (*10*). This strong scattering asymmetry results in different colors of the same nanoparticles when observed in the dark-field microscope in transmission or reflection mode (insets in Fig. 3E) (*10*). Suppression of the backward scattering was also observed for single GaAs nanodisks (*26*).

The interference effects between electric and magnetic dipole resonances of dielectric nanoparticles may have multiple applications, including efficient nanoantenna structures, Huygens metasurfaces, and unconventional Brewster angle behavior.

Dielectric nanoantennas

Light control at the nanoscale is important for many emerging applications, including 3D optical interconnects in multilayer chips, enhancement of fluorescence signals in bioimaging, high-resolution spatial light modulators, and light energy concentration in heat-assisted magnetic recording. At the subwavelength scale, conventional optical elements are not applicable, and nanoscale elements such as optical nanoantennas (*36*) offer a conceptually new approach for the design of nanoscale photonic devices. The study of nanoantennas is a rapidly growing area of research, and various geometries have been demonstrated successfully for nonclassical light emission, fluorescence enhancement, high-harmonic generation, nanoscale photodetectors, and single-molecule detection (*36*). Despite this progress, plasmonic nanoantennas working in optics are still far from attaining the same good characteristics as conventional antennas at radio frequencies, primarily because of losses in metallic elements. Therefore, all-dielectric nanoantennas are viewed as a reasonable alternative to plasmonic structures. At microwave frequencies, the so-called dielectric resonator antennas (*37*), made of ceramic components of various shapes, are commonly used. The use of dielectrics leads to many advantages such as low loss, small size, light weight, high radiation efficiency, and reasonable bandwidth. At optical frequencies, typical dielectrics may have low losses similar to those at microwave frequencies, but their refractive indices are limited to smaller numbers ($n \sim 4$), which imposes limitations on the size of the nanoantenna devices scaling proportionally to λ/n.

For a single-particle nanoantenna excited by a localized light source, the optimal conditions for the directional scattering differ from plane-wave excitation. They depend not only on the frequency but also on the relative distance between the source dipole and the nanoparticle (*38*). Thus, a single dielectric nanoparticle can either reflect or collect the light emitted by a photon source (*39*). The directivity can be tuned by controlling the distance between the emitter and the nanoparticle at the scale of $\lambda/6n$ (*38*). By using an array of nanoparticles, it is possible to enhance the overall directivity of optical nanoantennas, including the emission maximum (*38*) and direction (*40*), in more versatile ways. An all-dielectric analog of the well-known Yagi-Uda nanoantenna was shown to exhibit high directivity together with higher radiation efficiency than that of its plasmonic counterpart (*41*). This concept was verified experimentally in the microwave regime (*42*) by using spherical ceramic particles with a refractive index close to that of Si in the visible range.

Another important property of nanoantennas is their ability to concentrate electromagnetic energy at the nanoscale. Plasmonic nanoantennas may achieve high enhancement of the electric near-field while only weakly affecting the magnetic near-field. In contrast, resonant dielectric nanostructures not only can enhance electric near-fields (*43*, *44*) but can also behave like magnetic near-field concentrators. It was predicted theoretically (*45*) and demonstrated experimentally for microwaves (*46*) and visible wavelengths (*47*) that a dimer composed of two high-index dielectric nanoparticles with a subwavelength gap can enhance the magnetic field intensity by as much as two orders of magnitude. At the same time, the electric near-field intensity can also be enhanced (Fig. 4A). Magnetic hotspots, in addition to the electric hotspots, result in an increase of the local optical density of states, and thus can modify the magnetic transition rates of molecules or quantum emitters with an enhancement of the Purcell factor (*39*, *45*, *48*). The mode structure of dielectric dimer nanoantennas has been further investigated using spectroscopic (*49*) and cathodoluminescence (*50*) techniques. Recently, silicon dimers have been used for high surface-enhanced Raman scattering and surface-enhanced fluorescence without generating heat; nanoantennas using such components are suitable for detection of heat-sensitive biological species (*51*).

The overall scattering efficiency is also of prime importance. It was recently demonstrated that certain arrangements of nanoparticles, such

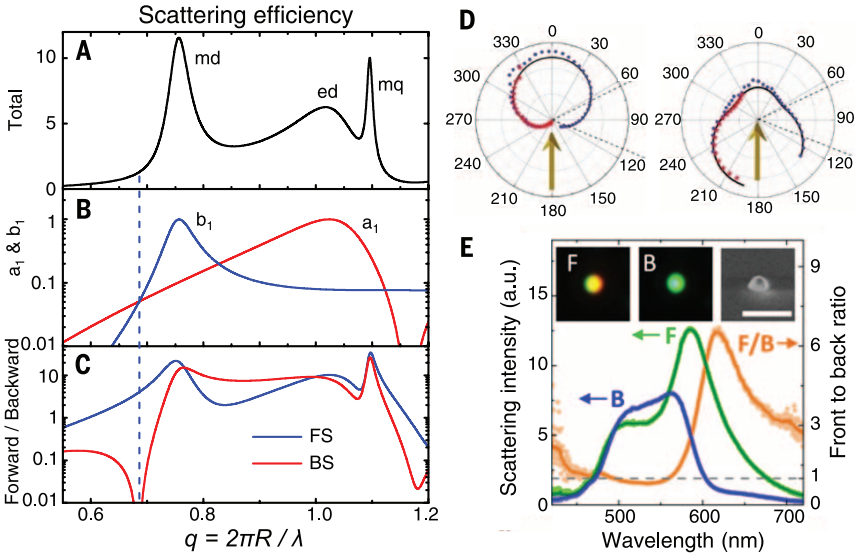

Fig. 3. Directional scattering of light by a single dielectric nanoparticle. (**A**) Scattering efficiency of a dielectric sphere calculated by Mie theory versus size parameter q for refractive index $n = 4$. Abbreviations for resonances are as in Fig. 1. (**B**) Electric a_1 and magnetic b_1 dipole scattering coefficients of the sphere (log scale). (**C**) Forward (FS) and backward (BS) scattering efficiencies of the sphere (log scale). The dashed line in (A) to (C) marks the wavelength at which the first Kerker condition is realized. (**D**) Experimental forward and backward scattering from a subwavelength spherical dielectric particle with diameter of 18 mm, recorded using a 3D angular measurement setup in the microwave spectral range at $\lambda = 84$ mm (left) and 69 mm (right). Dots are experimental data points; solid curves are Mie theory calculations (*35*). (**E**) Experimentally measured forward (green) and backward (blue) scattering spectra and forward-to-backward ratio (orange) of a near-spherical Si nanoparticle with a diameter of about 150 nm placed on a glass substrate (a.u., arbitrary units). Insets show transmission (F) and reflection (B) dark-field microscope images and a SEM image of the nanoparticle (*10*); scale bar for SEM image, 500 nm.

Downloaded from https://www.science.org at Moscow State University on March 10, 2022

as oligomers, can lead to resonant suppression of the total scattering efficiency, a phenomenon associated with Fano resonances (28, 29). A Fano resonance typically arises from the interference of broad and narrow spectral lines. In the case of plasmonic oligomers, most of the incident excitation is absorbed by nanoparticles. A new route for achieving Fano resonances in nanoparticle oligomers is now possible through the use of electric and magnetic resonances in lossless high-index dielectric nanoparticles (Fig. 4B) (52, 53). The origin of the observed Fano resonances is interference of the optically induced magnetic dipole mode of the central particle with the collective mode of the nanoparticle structure (52). Fano resonance can also be observed in simpler geometries such as an individual silicon nanostripe (54).

Because of their low losses and strong magnetic response, resonant dielectric nanoparticles offer a unique playground to demonstrate new nanophotonic effects. One of them is the existence of a nonradiating anapole (i.e., poleless) mode recently observed in silicon nanodisks. In classical electrodynamics, the anapole mode is strongly related to the existence of a toroidal dipole excitation. In general, the toroidal response is produced by currents flowing on the surface of a torus along its meridians (55). Despite a scale factor, the polarization and angular distribution of the radiated fields of the dynamic toroidal dipoles are exactly the same as those of conventional electric dipoles. As a result, a particular superposition of electric and toroidal dipole moments can cause the complete destructive interference of the corresponding far-field radiation contributions. Such a vanishing electromagnetic field produced by a nontrivial current source is a classical analog of the radiationless anapole initially introduced by Zel'dovich in nuclear physics. Interestingly, such peculiar induced currents can be naturally excited inside dielectric nanoparticles.

The anapole mode was recently demonstrated within an individual dielectric nanoparticle in the visible spectrum (56). In particular, a silicon nanodisk with a height of 50 nm and diameter of 310 nm was observed to exhibit a pronounced dip in the far-field scattering and a simultaneous near-field enhancement inside and around the disk (Fig. 4C) (56). These particles become nearly invisible in the far-field at the wavelength of anapole excitation. At the same time, the electric field energy is maximized inside the particles at the same wavelength; this was recently confirmed by third-harmonic generation experiments (57). Although the anapole in the dielectric nanodisks originates from mere interference, it provides new perspective for investigations into electromagnetic properties of various charge-current distributions.

Potential areas of application for low-loss dielectric nanoantennas not yet explored in the literature also include optoacoustics and elastodynamics.

Nonlinear optics with resonant dielectric nanostructures

Near-field enhancement of electric and magnetic response in all-dielectric nanostructures may lead to novel nonlinear effects. In particular, second- and third-harmonic generation (SHG and THG), self-action of light, and Raman scattering are affected by strong confinement resulting from geometrical resonances. Plasmonic resonances that enhance local electric fields in hotspots are known to boost nonlinear optical effects in metal nanostructures. In contrast to plasmonics, resonances of high-index dielectric nanoparticles provide a mode volume that is not limited to interfaces and thus may lead to higher conversion efficiencies.

The enhanced THG from Si nanodisks exhibiting both electric and magnetic dipole resonances was observed experimentally (58) through third-harmonic microscopy and spectroscopy, with the TH signal enhanced in the vicinity of the magnetic dipole resonance (Fig. 4D). The field localization at the magnetic resonance results in an enhancement of the harmonic intensity by two orders of magnitude with respect to unstructured bulk Si, with the conversion efficiency limited only by the two-photon absorption in the substrate (58). Strong THG has also been reported from Si-based metasurfaces (59). Combining the Kerr effect with a high–quality factor resonance in the metasurface linear transmittance

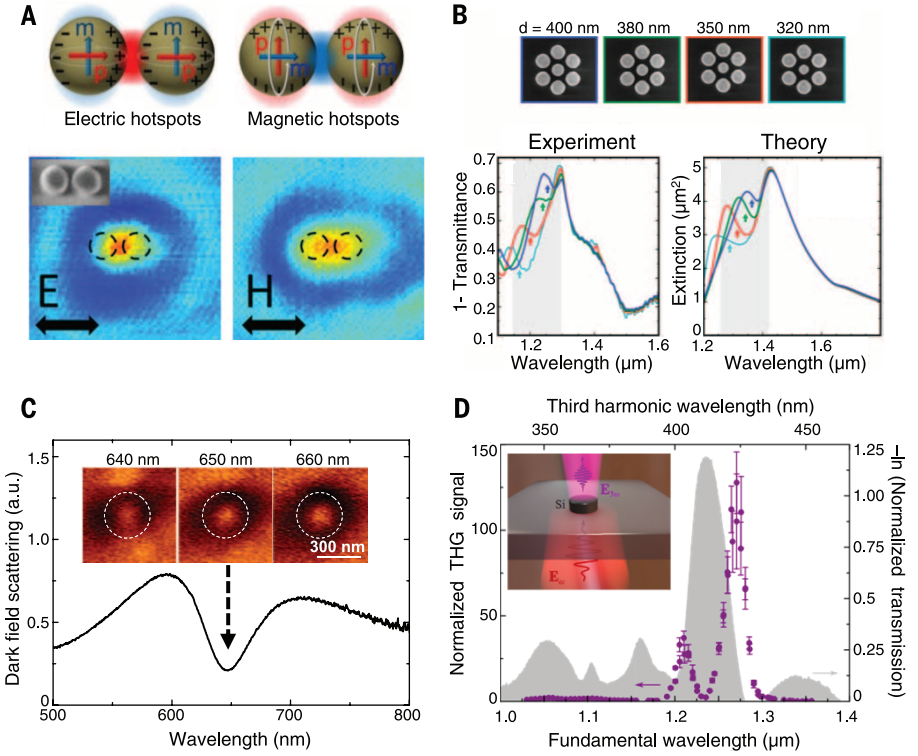

Fig. 4. Dielectric nanoantennas. (**A**) Magnetic and electric near-field enhancement in a nanogap between two silicon nanocylinders (height, 150 nm; diameter, 140 nm; gap, 30 nm). Top: Schematics of the measured system; p and m indicate electric and magnetic dipole moments, respectively. Bottom: Scanning near-field optical microscopy images for the two orthogonal excitation polarizations (47). Arrows indicate polarization direction for electric (**E**) and magnetic (**H**) fields. Color varies from minimal (blue) to maximal (red) values. Dashed circles mark the positions of silicon nanocylinders. Inset shows a SEM image of the studied dimer nanoantenna. (**B**) Magnetic Fano resonance in all-dielectric oligomers (53). Top: SEM images of fabricated heptamer for different diameters (d) of the central Si disk. Bottom: Theoretical and experimental demonstrations of the magnetic Fano resonances. Blue, green, red, and cyan curves correspond to different diameters of the central Si nanodisk: 400 nm, 380 nm, 350 nm, and 320 nm, respectively. Arrows indicate the spectral positions of the Fano resonance. (**C**) Nonradiating anapole mode in silicon nanodisks (56): Experimental dark-field scattering spectra of an amorphous Si nanodisk (diameter, 310 nm; height, 50 nm) on a quartz substrate. A strong dip in the nanodisk scattering at the wavelength of anapole excitation is clearly observed. Inset shows experimental near-field scanning optical microscopy images of the anapole mode at three different wavelengths (640, 650, and 660 nm) near the scattering minimum. White dashed circles indicate the nanodisks' positions. (**D**) Nonlinear spectroscopy of an array of Si nanodisks (58). Shown is the negative logarithm of the normalized transmission spectrum of a sample marked by a gray area indicating a resonance at 1.24 μm. The third-harmonic generation (THG) spectrum of the sample normalized over the spectrum of the substrate (purple dots) is strongly enhanced within the spectral band of the resonance. The inset shows a schematic of the THG at a single silicon nanodisk.

Downloaded from https://www.science.org at Moscow State University on March 10, 2022

spectrum, the authors demonstrated THG conversion efficiency of 1.18×10^{-6} at a peak pump intensity of 3.2 GW/cm^2. This corresponds to 1.5×10^5 enhancement of the THG signal relative to that from an unstructured Si film with the same thickness. Recent demonstrations also include enhancement of SHG in resonant nanopillars made of the high-index noncentrosymmetric III-V semiconductors GaAs (*60*) and AlGaAs (*61*). An enhancement factor of 10^4 relative to unstructured GaAs films is shown with total conversion efficiency of 2×10^{-5} at a pump intensity of 3.4 GW/cm^2. Strong quadratic nonlinear processes pave the way for the enhanced generation of entangled photon pairs through spontaneous parametric downconversion (SPDC) with dielectric nanoresonators and experimental realization of nanoscale quantum-entangled light sources that use optical nonlinearity.

Apart from the harmonic generation, efficient tuning of optical properties of high-index nanoparticles near magnetic Mie-type resonances by means of femtosecond laser irradiation has also been demonstrated (*62*). The effect is based on ultrafast (<100 fs) photoinjection of dense electron-hole plasma within such nanoparticles, drastically changing their transient dielectric permittivity. Reflectance changes up to 20% have been achieved. In a similar experiment, ultrafast all-optical switching in subwavelength nonlinear dielectric nanostructures exhibiting localized magnetic resonances has been shown (*63*). Pump-probe measurements have revealed that switching in the nanodisks can be governed by pulse-limited 65-fs two-photon absorption, which is enhanced by a factor of 80 with respect to the unstructured silicon film (*63*).

These experimental demonstrations indicate great promise for the rapidly developing field of nonlinear and quantum nanophotonics. The main advantage of resonant dielectric nanostructures over plasmonics is the localization and strong enhancement of optical fields inside the particles, which promotes strong volumetric nonlinearities and allows for large conversion efficiencies.

Metamaterials and metasurfaces based on resonant dielectric nanostructures

Electromagnetic properties of media composed of resonant dielectric scatterers were discussed in many theoretical works starting from Lewin (*64*). Magnetic response of purely dielectric particles with very high refractive index (close to 50) was also studied theoretically (*65*). During the previous decade, this problem was reconsidered in connection to metamaterials (*16*, *66*, *67*). Some earlier theoretical results, as well as the first experimental demonstrations of such composite media at gigahertz frequencies, are reviewed in (*68*). In the visible and near-IR spectral ranges, practical materials such as Si and germanium (Ge) have the highest refractive index, around 4, which is substantially lower than the values available at microwave frequencies. Therefore, 3D periodic structures composed of such nanoparticles should demonstrate the properties of photonic crystals and are not suitable for the homogenization of parameters (*69*), with the exception of zero-index materials (*70*).

Resonant dielectric nanoparticles can also be used for creating planar single-layer arrays known as metasurfaces (*71*). Metasurfaces offer the possibility of engineered resonant electric and magnetic optical response combined with low losses of thin-layer structures, and hence they demonstrate many useful properties of metadevices. One of the major functionalities of metasurfaces is control of the phase of reflected and transmitted light. The idea of using dielectrics structured at the subwavelength scale for wavefront control was actively discussed two decades ago in the context of blazing gratings (*72*). Similar ideas have also been pursued more recently (*73*–*76*) to achieve the 2π phase accumulation. This approach does not directly rely on resonances of single elements and requires relatively tall nanopillars (on the order of a free-space wavelength) and a high aspect ratio, sometimes reaching 10:1. At the same time, it provides the highest efficiencies to date for operation in the transmission mode, in the range of 80 to 90%.

Another approach to achieving phase control was proposed in the early 2000s, and it relies on metallic or dielectric subwavelength gratings with different orientations to control the circularly polarized light through a geometric Pancharatnam-Berry (PB) phase (*77*, *78*). A recent work based on this principle demonstrated flat silicon lenses and axicons operating at visible wavelengths (Fig. 5A) (*79*). The structure is generated by patterning 120-nm-wide nanoantennas into a 100-nm-thick Si film. It could be reduced in thickness relative to previous PB-phase elements by exploiting resonances in the Si structures. This approach was further extended to highly efficient operation at visible wavelengths by using transparent titanium dioxide (TiO_2) as the metasurface material (*80*). Beam focusing with efficiency of >66% at selected wavelengths in blue, red, and green regions has been experimentally demonstrated. In contrast to the previous example, this design was achieved with a relatively large height of TiO_2 structures (600 nm), which imposes greater restrictions on the nanofabrication.

A novel approach to creating dielectric metasurfaces is to use electric and magnetic dipole resonances of dielectric nanoparticles to control the phase of incoming light (*81*). Each of the dipoles is capable of shifting the phase from 0 to π near the resonance. Combining the response of both dipoles at the same wavelength makes it possible to achieve the whole 0 to 2π phase coverage (*82*). This overlap of resonances provides not only the required phase shifts but also near-unity transmission of the metasurface, due to the

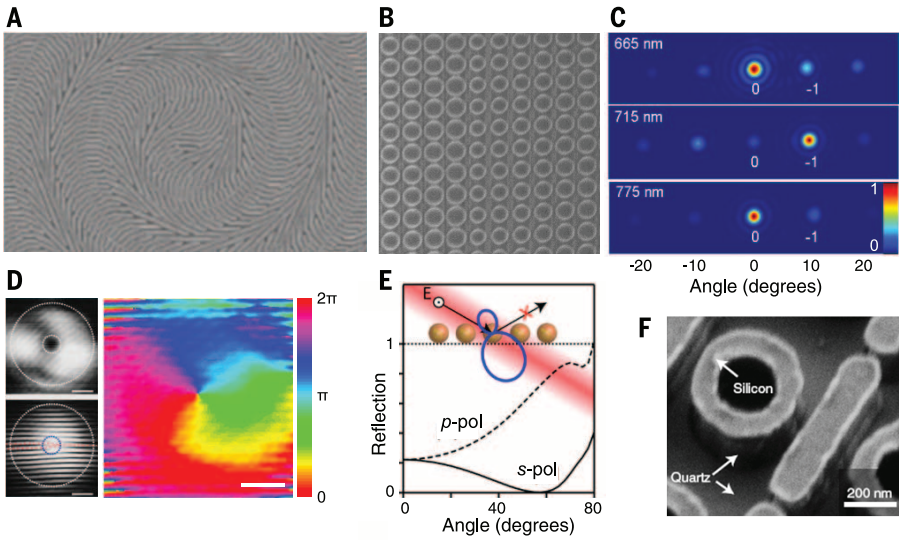

Fig. 5. Dielectric metasurfaces. (**A**) SEM image of a dielectric metasurface constructed from >10^4 Si nanoantennas and serving as an optical axicon (*79*). (**B** and **C**) Beam deflection with a Huygens silicon metasurface (*84*): (B) SEM image of a 130-nm-thick gradient resonant metasurface; (C) back focal plane image of light transmitted through the metasurface showing close to 50% total deflection efficiency at 715 nm. "0" and "−1" labels indicate the angular positions of the corresponding diffraction orders. (**D**) Vortex beam generated by a Huygens dielectric metasurface in transmission (*85*). Left: Logarithmic intensity profile of the generated vortex beam (top); interferogram showing the characteristic fork structure (bottom). Right: Reconstructed phase of the vortex beam imaged at 4 cm beyond the sample. All scale bars are 200 μm. (**E**) Demonstration of the generalized Brewster effect with a silicon metasurface. Simulated reflection of p- and s-polarized light at a wavelength of 710 nm from a square array of silicon spheres with diameter of 180 nm and pitch of 300 nm shows Brewster angle behavior for s polarization. Inset at top illustrates how electric and magnetic dipoles interfere to cancel the reflection of s-polarized incident light through scattering cancellation in the reflection direction (*90*). (**F**) SEM image of a unit cell of the silicon metasurface, demonstrating electromagnetically induced transparency behavior in the near-IR spectral range (*92*).

Downloaded from https://www.science.org at Moscow State University on March 10, 2022

enhanced forward scattering by each of the nanoparticles, and suppression of backward scattering, due to the first Kerker condition. Such designs are conceptually similar to Huygens metasurfaces proposed in plasmonics (*83*), but they have much higher transmission efficiencies due to lower losses in transparent dielectric materials. Recently, silicon-based visible-range metasurfaces with resonant transmission greater than 85% have been experimentally demonstrated (*84*). These devices are only 130 nm thick, corresponding to less than one-fifth of the free-space wavelength, and are capable of controlling the wavefront of light and performing beam deflection with close to 50% efficiency in transmission (Fig. 5, B and C). Similar concepts were also used to achieve efficient vortex beam generation (*85*, *86*) (Fig. 5D). Because of the low thickness and low aspect ratio of the nanodisks (around 1:2), this approach, despite slightly lower efficiency, might be promising for practical applications relying on large-scale nanofabrication techniques such as nanoimprinting.

Apart from transmission phase manipulation, dielectric metasurfaces can also be used as almost perfect reflectors exceeding the performance of conventional metallic and dielectric mirrors (*6*, *24*, *87*). In contrast to high-transmissivity arrays, which are based on disks with an aspect ratio of approximately 1:2 and have overlapped electric and magnetic dipole resonances, high reflectance can be achieved with spheres or cylinders with an aspect ratio close to 1:1, whose electric and magnetic dipole resonances are spectrally separated. This effect arises from the coherent interaction of magnetic or electric dipoles excited by an external radiation in each nanoparticle. A recent experiment demonstrated very high reflectance (up to 99.7%) in the near-IR spectral range from a dense array of Si nanoparticles (*24*). This high-reflectance behavior is conceptually similar to that observed earlier in high-contrast subwavelength gratings [see (*88*) and references therein].

Interfering electric and magnetic dipoles may lead to phenomena that cannot be observed with conventional dielectrics or metals. One such effect is magnetic mirror–like behavior, when the dielectric metasurface acts as a perfect magnetic conductor flipping the phase of an incident magnetic field with no effect on the phase of the electric field (*89*). Another example is the generalized Brewster effect (*90*). In contrast to the conventional Brewster effect, which is limited to p-polarized incidence and angles above 45° (a Brewster angle below 45° is always accompanied by total internal reflection at higher angles), the generalized Brewster effect can be achieved for any polarization (both p and s) and any angle of incidence (both below and above 45° without having total internal reflection) (Fig. 5E). It appears as a result of interference of electric and magnetic resonances in the array and cancellation of their scattering in the reflection direction.

Another approach to dielectric metasurfaces is to use dielectrics for the plasmonic-inspired designs with a substantial reduction of losses. Examples are the spectrally selective Fano metasurfaces (*91*) and metasurface analogs of electromagnetically induced transparency (*92*) (Fig. 5F). In the latter case, because of extremely low absorption loss and coherent interaction of neighboring nanoparticles, a resonance quality factor of 483 is observed, leading to a refractive index sensor with a figure of merit of 103. Furthermore, it was shown that dielectric metasurfaces can be engineered to confine the optical field in either the Si resonator or the environment, allowing one to tailor light-matter interaction at the nanoscale (*92*).

Dielectric metasurfaces hold promise for real-world applications to novel ultracompact optical components and wearable photonic devices because of their high efficiency, ease of fabrication, and CMOS compatibility. A key to their success may lie in development of their broadband operation and active switching capabilities. Recent experimental demonstrations of a silicon metasurface operating at three different wavelengths (*93*), active tuning of the spectral position of dielectric metasurface resonances by liquid crystals (*94*), and theoretical prediction of the retardation phase tunability of InSb metasurfaces by charge injection (*95*) are the first important steps in this direction.

The field of dielectric metamaterials is developing very rapidly. Additional information related to zero-index and anisotropic all-dielectric metamaterials can be found in (*96*).

Optoelectronic devices using resonant semiconductor nanostructures

Advances in nanotechnology and semiconductor electronics enable the realization of complex device architectures constructed from nanoscale semiconductor elements. This progress has opened up tremendous opportunities for nanophotonics because at this size scale, the semiconductor structures naturally possess optical resonances that can be used to manipulate light-material interactions for a wide range of applications. Although the study of resonances in high-index nanostructures has a long history, only recently have researchers started to use these resonances to enhance the performance of optoelectronic devices such as photodetectors (*97*–*99*), optical sources (*100*), and thermal emitters based on individual nanostructures (*101*), as well as large-area nanostructured devices such as solar cells (*23*, *102*–*105*) and photoelectrochemical devices (*106*).

Figure 6A shows a single semiconductor nanowire photodetector that capitalizes on its optical resonances to achieve an absorption cross section σ_{abs} that exceeds its geometric cross section σ_{geom} (*97*, *98*). The high absorption efficiency $Q_{abs} = \sigma_{abs}/\sigma_{geom}$ enables more efficient, high-speed, low-noise photodetection schemes. Photocurrent spectra taken from single Ge nanowire detectors with different radii show peaks that are not visible in the intrinsic materials absorption of Ge and are attributed to the excitation of optical resonances that enhance absorption (Fig. 6B). These spectra qualitatively agree well with the predicted absorption features of Ge nanowires with the corresponding radii (Fig. 6C) in terms of the number of absorption peaks and their spectral location. Conversely, it has also been

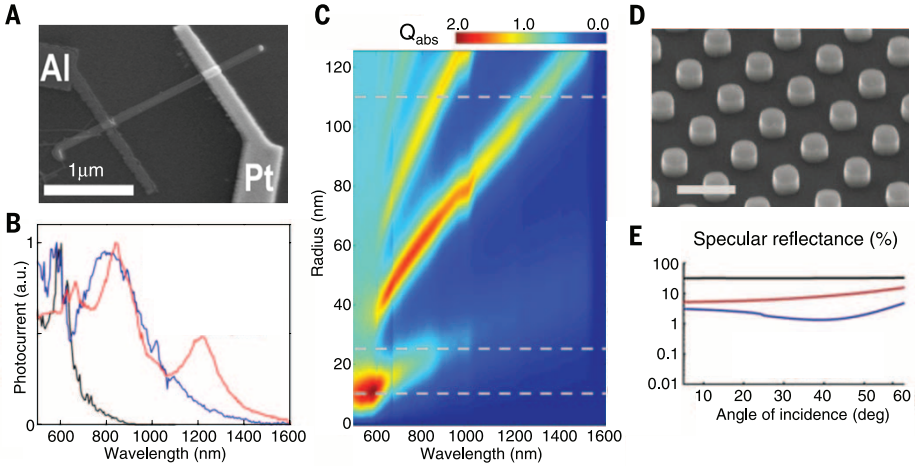

Fig. 6. Nanophotonic devices based on semiconductor nanoantennas. (**A**) SEM image of a photodetector using an optically resonant Ge nanowire with asymmetric metallic contacts [one side ohmic (Al), the other side Schottky (Pt)] (*98*). (**B**) Photocurrent spectra of individual Ge nanowires with radii of 10 nm (black), 25 nm (blue), and 110 nm (red) (*97*). (**C**) Two-dimensional plot of the calculated absorption efficiency Q_{abs} as a function of wavelength and radius of the nanowire. The dashed gray lines indicate the radii for which the spectral photocurrent is shown in (B) (*97*). (**D**) SEM image of an array of Si Mie resonators that serves as an antireflection coating on a Si substrate (*23*). Scale bar, 1 μm. (**E**) Measurement of the specular reflectance at 632 nm as a function of the angle of incidence for a bare Si wafer (black), a 60-nm-thick Si_3N_4 antireflection coating (red), and an array of Mie resonators as shown in (D) coated with a 60-nm-thick Si_3N_4 layer (blue) (*23*).

Downloaded from https://www.science.org at Moscow State University on March 10, 2022

demonstrated that subwavelength structures can emit via their size-tunable resonances, affording new levels of control over the spectral emission (*100*, *101*).

Large arrays of Mie resonators can also be realized on top of devices—for example, as a high-performance antireflection coating (Fig. 6, D and E) (*23*). Here, the Mie resonators can assist in increasing the flow of light into a high-index solar cell. Alternatively, a layer of judiciously shaped Mie resonators can be used to create ultrathin metafilms with designer absorption spectra (*107*). From a device perspective, some key advantages of resonant semiconductors over metals are the natural materials compatibility with semiconductor device technology, the longer lifetimes of excited carriers, an ability to electrically gate carrier densities, and the possibility of defining device functions (such as p-n junctions) inside the resonant structures.

Further developments and outlook

Because of their unique optically induced electric and magnetic resonances, high-index dielectric nanostructures are expected to complement or even replace plasmonic components in a range of potential applications. The unique low-loss resonant behavior makes it possible to realize many subwavelength resonant effects demonstrated in nanophotonics without much energy dissipation into heat. In addition, the coexistence of strong electric and magnetic resonances, their interference, and the resonant enhancement of the magnetic field in dielectric nanoparticles bring entirely new functionalities to simple geometries largely unexplored in plasmonic structures, especially in the nonlinear and quantum regimes.

In the visible range, the main materials of choice are silicon, germanium, TiO_2, GaAs, and other semiconductors with high values of the optical refractive index. These materials are extensively used in current device technologies, enabling many novel functionalities offered by the subwavelength physics of high-index resonant dielectric nanostructures to be transferred directly into existing industrial production lines.

REFERENCES AND NOTES

1. L. Novotny, B. Hecht, *Principles of Nano-optics* (Cambridge Univ. Press, 2012).
2. A. Boltasseva, H. A. Atwater, Low-loss plasmonic metamaterials. *Science* **331**, 290–291 (2011). doi: 10.1126/science.1198258; pmid: 21252335
3. C. F. Bohren, D. R. Huffman, *Absorption and Scattering of Light by Small Particles* (Wiley, 1983).
4. J. B. Pendry, A. J. Holden, D. J. Robbins, W. J. Stewart, Magnetism from conductors and enhanced nonlinear phenomena. *IEEE Trans. Microw. Theory Tech.* **47**, 2075–2084 (1999). doi: 10.1109/22.798002
5. J. A. Schuller, M. L. Brongersma, General properties of dielectric optical antennas. *Opt. Express* **17**, 24084–24095 (2009). doi: 10.1364/OE.17.024084; pmid: 20052120
6. A. B. Evlyukhin, C. Reinhardt, A. Seidel, B. S. Luk'yanchuk, B. N. Chichkov, Optical response features of Si-nanoparticle arrays. *Phys. Rev. B* **82**, 045404 (2010). doi: 10.1103/PhysRevB.82.045404
7. A. García-Etxarri *et al.*, Strong magnetic response of submicron silicon particles in the infrared. *Opt. Express* **19**, 4815–4826 (2011). doi: 10.1364/OE.19.004815; pmid: 21445117
8. A. I. Kuznetsov, A. E. Miroshnichenko, Y. H. Fu, J. Zhang, B. Luk'yanchuk, Magnetic light. *Sci. Rep.* **2**, 492 (2012). doi: 10.1038/srep00492; pmid: 22768382
9. Y. Zhang, M. Nieto-Vesperinas, J. J. Sáenz, Dielectric spheres with maximum forward scattering and zero backscattering: A search for their material composition. *J. Opt.* **17**, 105612 (2015). doi: 10.1088/2040-8978/17/10/105612
10. Y. H. Fu, A. I. Kuznetsov, A. E. Miroshnichenko, Y. F. Yu, B. Luk'yanchuk, Directional visible light scattering by silicon nanoparticles. *Nat. Commun.* **4**, 1527 (2013). doi: 10.1038/ncomms2538; pmid: 23443555
11. B. S. Luk'yanchuk, N. V. Voshchinnikov, R. Paniagua-Dominguez, A. I. Kuznetsov, Optimum forward light scattering by spherical and spheroidal dielectric nanoparticles with high refractive index. *ACS Photonics* **2**, 993–999 (2015). doi: 10.1021/acsphotonics.5b00261
12. A. B. Evlyukhin, C. Reinhardt, B. N. Chichkov, Multipole light scattering by nonspherical nanoparticles in the discrete dipole approximation. *Phys. Rev. B* **84**, 235429 (2011). doi: 10.1103/PhysRevB.84.235429
13. M. A. van de Haar, J. van de Groep, B. J. M. Brenny, A. Polman, Controlling magnetic and electric dipole modes in hollow silicon nanocylinders. *Opt. Express* **24**, 2047–2064 (2016). doi: 10.1364/OE.24.002047; pmid: 26906780
14. J. Zhang, K. F. MacDonald, N. I. Zheludev, Near-infrared trapped mode magnetic resonance in an all-dielectric metamaterial. *Opt. Express* **21**, 26721–26728 (2013). doi: 10.1364/OE.21.026721; pmid: 24216893
15. I. Staude *et al.*, Tailoring directional scattering through magnetic and electric resonances in subwavelength silicon nanodisks. *ACS Nano* **7**, 7824–7832 (2013). doi: 10.1021/nn402736f; pmid: 23952969
16. J. A. Schuller, R. Zia, T. Taubner, M. L. Brongersma, Dielectric metamaterials based on electric and magnetic resonances of silicon carbide particles. *Phys. Rev. Lett.* **99**, 107401 (2007). doi: 10.1103/PhysRevLett.99.107401; pmid: 17930407
17. L. Cao, P. Fan, E. S. Barnard, A. M. Brown, M. L. Brongersma, Tuning the color of silicon nanostructures. *Nano Lett.* **10**, 2649–2654 (2010). doi: 10.1021/nl1013794; pmid: 20507083
18. G. Brönstrup *et al.*, Optical properties of individual silicon nanowires for photonic devices. *ACS Nano* **4**, 7113–7122 (2010). doi: 10.1021/nn101076t; pmid: 21080685
19. K. Seo *et al.*, Multicolored vertical silicon nanowires. *Nano Lett.* **11**, 1851–1856 (2011). doi: 10.1021/nl200201b; pmid: 21413684
20. A. B. Evlyukhin *et al.*, Demonstration of magnetic dipole resonances of dielectric nanospheres in the visible region. *Nano Lett.* **12**, 3749–3755 (2012). doi: 10.1021/nl301594s; pmid: 22703443
21. A. I. Kuznetsov, J. Koch, B. N. Chichkov, Laser-induced backward transfer of gold nanodroplets. *Opt. Express* **17**, 18820–18825 (2009). doi: 10.1364/OE.17.018820; pmid: 20372615
22. U. Zywietz, A. B. Evlyukhin, C. Reinhardt, B. N. Chichkov, Laser printing of silicon nanoparticles with resonant optical electric and magnetic responses. *Nat. Commun.* **5**, 3402 (2014). doi: 10.1038/ncomms4402; pmid: 24595073
23. P. Spinelli, M. A. Verschuuren, A. Polman, Broadband omnidirectional antireflection coating based on subwavelength surface Mie resonators. *Nat. Commun.* **3**, 692 (2012). doi: 10.1038/ncomms1691; pmid: 22353722
24. P. Moitra *et al.*, Large-scale all-dielectric metamaterial perfect reflectors. *ACS Photonics* **2**, 692–698 (2015). doi: 10.1021/acsphotonics.5b00148
25. L. Shi *et al.*, Monodisperse silicon nanocavities and photonic crystals with magnetic response in the optical region. *Nat. Commun.* **4**, 1904 (2013). doi: 10.1038/ncomms2934; pmid: 23695698
26. S. Person *et al.*, Demonstration of zero optical backscattering from single nanoparticles. *Nano Lett.* **13**, 1806–1809 (2013). doi: 10.1021/nl4005018; pmid: 23461654
27. J. C. Ginn *et al.*, Realizing optical magnetism from dielectric metamaterials. *Phys. Rev. Lett.* **108**, 097402 (2012). doi: 10.1103/PhysRevLett.108.097402; pmid: 22463666
28. B. Luk'yanchuk *et al.*, The Fano resonance in plasmonic nanostructures and metamaterials. *Nat. Mater.* **9**, 707–715 (2010). doi: 10.1038/nmat2810; pmid: 20733610
29. A. E. Miroshnichenko, S. Flach, Y. S. Kivshar, Fano resonances in nanoscale structures. *Rev. Mod. Phys.* **82**, 2257–2298 (2010). doi: 10.1103/RevModPhys.82.2257
30. M. Nieto-Vesperinas, R. Gómez-Medina, J. J. Sáenz, Angle-suppressed scattering and optical forces on submicrometer dielectric particles. *J. Opt. Soc. Am. A* **28**, 54–60 (2011). doi: 10.1364/JOSAA.28.000054; pmid: 21200411
31. R. Gómez-Medina *et al.*, Electric and magnetic dipolar response of germanium nanospheres: Interference effects, scattering anisotropy, and optical forces. *J. Nanophotonics* **5**, 053512 (2011). doi: 10.1117/1.3603941
32. M. Kerker, D. Wang, G. Giles, Electromagnetic scattering by magnetic spheres. *J. Opt. Soc. Am.* **73**, 765–767 (1983). doi: 10.1364/JOSA.73.000765
33. A. Alu, N. Engheta, How does zero forward-scattering in magnetodielectric nanoparticles comply with the optical theorem? *J. Nanophotonics* **4**, 041590 (2010). doi: 10.1117/1.3449103
34. B. García-Cámara, J. M. Saiz, F. González, F. Moreno, Nanoparticles with unconventional scattering properties: Size effects. *Opt. Commun.* **283**, 490–496 (2010). doi: 10.1016/j.optcom.2009.10.027
35. J. M. Geffrin *et al.*, Magnetic and electric coherence in forward- and back-scattered electromagnetic waves by a single dielectric subwavelength sphere. *Nat. Commun.* **3**, 1171 (2012). doi: 10.1038/ncomms2167; pmid: 23132021
36. L. Novotny, N. van Hulst, Antennas for light. *Nat. Photonics* **5**, 83–90 (2011). doi: 10.1038/nphoton.2010.237
37. R. K. Mongia, P. Bhartia, Dielectric resonator antennas—a review and general design relations for resonant frequency and bandwidth. *Int. J. Microwave Mill.* **4**, 230–247 (1994).
38. B. Rolly, B. Stout, N. Bonod, Boosting the directivity of optical antennas with magnetic and electric dipolar resonant particles. *Opt. Express* **20**, 20376–20386 (2012). doi: 10.1364/OE.20.020376; pmid: 23037088
39. M. K. Schmidt *et al.*, Dielectric antennas—a suitable platform for controlling magnetic dipolar emission. *Opt. Express* **20**, 13636–13650 (2012). doi: 10.1364/OE.20.013636; pmid: 22714428
40. L. Zou *et al.*, Dielectric resonator nanoantennas at visible frequencies. *Opt. Express* **21**, 1344–1352 (2013). doi: 10.1364/OE.21.001344; pmid: 23389028
41. A. E. Krasnok, A. E. Miroshnichenko, P. A. Belov, Y. S. Kivshar, All-dielectric optical nanoantennas. *Opt. Express* **20**, 20599–20604 (2012). doi: 10.1364/OE.20.020599
42. D. S. Filonov *et al.*, Experimental verification of the concept of all-dielectric nanoantennas. *Appl. Phys. Lett.* **100**, 201113 (2012). doi: 10.1063/1.4719209
43. S. Hayashi, R. Koh, Y. Ichiyama, K. Yamamoto, Evidence for surface-enhanced Raman scattering on nonmetallic surfaces: Copper phthalocyanine molecules on GaP small particles. *Phys. Rev. Lett.* **60**, 1085–1088 (1988). doi: 10.1103/PhysRevLett.60.1085; pmid: 10037937
44. M. M. Sigalas, D. A. Fattal, R. S. Williams, S. Y. Wang, R. G. Beausoleil, Electric field enhancement between two Si microdisks. *Opt. Express* **15**, 14711–14716 (2007). doi: 10.1364/OE.15.014711; pmid: 19550752
45. P. Albella *et al.*, Low-loss electric and magnetic field-enhanced spectroscopy with subwavelength silicon dimers. *J. Phys. Chem. C* **117**, 13573–13584 (2013). doi: 10.1021/jp4027018
46. G. Boudarham, R. Abdeddaim, N. Bonod, Enhancing the magnetic field intensity with a dielectric gap antenna. *Appl. Phys. Lett.* **104**, 021117 (2014). doi: 10.1063/1.4861166
47. R. M. Bakker *et al.*, Magnetic and electric hotspots with silicon nanodimers. *Nano Lett.* **15**, 2137–2142 (2015). doi: 10.1021/acs.nanolett.5b00128; pmid: 25686205
48. B. Rolly, B. Bebey, S. Bidault, B. Stout, N. Bonod, Promoting magnetic dipolar transition in trivalent lanthanide ions with lossless Mie resonances. *Phys. Rev. B* **85**, 245432 (2012). doi: 10.1103/PhysRevB.85.245432
49. U. Zywietz *et al.*, Electromagnetic resonances of silicon nanoparticle dimers in the visible. *ACS Photonics* **2**, 913–920 (2015). doi: 10.1021/acsphotonics.5b00105
50. J. van de Groep, T. Coenen, S. A. Mann, A. Polman, Direct imaging of hybridized eigenmodes in coupled silicon nanoparticles. *Optica* **3**, 93–99 (2016). doi: 10.1364/OPTICA.3.000093
51. M. Caldarola *et al.*, Non-plasmonic nanoantennas for surface enhanced spectroscopies with ultra-low heat conversion. *Nat. Commun.* **6**, 7915 (2015). doi: 10.1038/ncomms8915; pmid: 26238815
52. A. E. Miroshnichenko, Y. S. Kivshar, Fano resonances in all-dielectric oligomers. *Nano Lett.* **12**, 6459–6463 (2012). doi: 10.1021/nl303927q; pmid: 23170879
53. K. E. Chong *et al.*, Observation of Fano resonances in all-dielectric nanoparticle oligomers. *Small* **10**, 1985–1990 (2014). doi: 10.1002/smll.201303612; pmid: 24616191

Downloaded from https://www.science.org at Moscow State University on March 10, 2022

54. P. Fan, Z. Yu, S. Fan, M. L. Brongersma, Optical Fano resonance of an individual semiconductor nanostructure. *Nat. Mater.* **13**, 471–475 (2014). doi: 10.1038/nmat3927; pmid: 24747781
55. N. Papasimakis, V. A. Fedotov, V. Savinov, T. A. Raybould, N. I. Zheludev, Electromagnetic toroidal excitations in matter and free space. *Nat. Mater.* **15**, 263–271 (2016). doi: 10.1038/nmat4563; pmid: 26906961
56. A. E. Miroshnichenko *et al*., Nonradiating anapole modes in dielectric nanoparticles. *Nat. Commun.* **6**, 8069 (2015). doi: 10.1038/ncomms9069; pmid: 26311109
57. G. Grinblat, Y. Li, M. P. Nielsen, R. F. Oulton, S. A. Maier, Enhanced third harmonic generation in single germanium nanodisks excited at the anapole mode. *Nano Lett.* **16**, 4635–4640 (2016). doi: 10.1021/acs.nanolett.6b01958; pmid: 27331867
58. M. R. Shcherbakov *et al*., Enhanced third-harmonic generation in silicon nanoparticles driven by magnetic response. *Nano Lett.* **14**, 6488–6492 (2014). doi: 10.1021/nl503029j; pmid: 25322350
59. Y. Yang *et al*., Nonlinear Fano-resonant dielectric metasurfaces. *Nano Lett.* **15**, 7388–7393 (2015). doi: 10.1021/acs.nanolett.5b02802; pmid: 26501777
60. S. Liu *et al*., Resonantly enhanced second-harmonic generation using III-V semiconductor all-dielectric metasurfaces. *Nano Lett.* **16**, 5426–5432 (2016). doi: 10.1021/acs.nanolett.6b01816; pmid: 27501472
61. V. F. Gili *et al*., Monolithic AlGaAs second-harmonic nanoantennas. *Opt. Express* **24**, 15965–15971 (2016). doi: 10.1364/OE.24.015965; pmid: 26259100
62. S. Makarov *et al*., Tuning of magnetic optical response in a dielectric nanoparticle by ultrafast photoexcitation of dense electron-hole plasma. *Nano Lett.* **15**, 6187–6192 (2015). doi: 10.1021/acs.nanolett.5b02534; pmid: 26259100
63. M. R. Shcherbakov *et al*., Ultrafast all-optical switching with magnetic resonances in nonlinear dielectric nanostructures. *Nano Lett.* **15**, 6985–6990 (2015). doi: 10.1021/acs.nanolett.5b02989; pmid: 26393983
64. L. Lewin, The electrical constants of a material loaded with spherical particles. *Proc. Inst. Electr. Eng.* **94**, 65–68 (1947).
65. G. Videen, W. S. Bickel, Light-scattering resonances in small spheres. *Phys. Rev. A* **45**, 6008–6012 (1992). doi: 10.1103/PhysRevA.45.6008; pmid: 9907700
66. S. O'Brien, J. B. Pendry, Photonic bandgap effects and magnetic activity in dielectric composites. *J. Phys. Condens. Matter* **14**, 4035–4044 (2002). doi: 10.1088/0953-8984/14/15/317
67. C. L. Holloway, E. F. Kuester, J. Baker-Jarvis, P. Kabos, A double negative (DNG) composite medium composed of magnetodielectric spherical particles embedded in a matrix. *IEEE Trans. Antenn. Propag.* **51**, 2596–2603 (2003). doi: 10.1109/TAP.2003.817563
68. Q. Zhao, J. Zhou, F. Zhang, D. Lippens, Mie resonance-based dielectric metamaterials. *Mater. Today* **12**, 60–69 (2009). doi: 10.1016/S1369-7021(09)70318-9
69. M. V. Rybin *et al*., Phase diagram for the transition from photonic crystals to dielectric metamaterials. *Nat. Commun.* **6**, 10102 (2015). doi: 10.1038/ncomms10102; pmid: 26626302
70. P. Moitra *et al*., Realization of an all-dielectric zero-index optical metamaterial. *Nat. Photonics* **7**, 791–795 (2013). doi: 10.1038/nphoton.2013.214
71. N. Yu, F. Capasso, Flat optics with designer metasurfaces. *Nat. Mater.* **13**, 139–150 (2014). doi: 10.1038/nmat3839; pmid: 24452357
72. P. Lalanne, S. Astilean, P. Chavel, E. Cambril, H. Launois, Design and fabrication of blazed binary diffractive elements with sampling periods smaller than the structural cutoff. *J. Opt. Soc. Am. A* **16**, 1143 (1999). doi: 10.1364/JOSAA.16.001143
73. E. Schonbrun, K. Seo, K. B. Crozier, Reconfigurable imaging systems using elliptical nanowires. *Nano Lett.* **11**, 4299–4303 (2011). doi: 10.1021/nl202324s; pmid: 21923112
74. P. R. West *et al*., All-dielectric subwavelength metasurface focusing lens. *Opt. Express* **22**, 26212–26221 (2014). doi: 10.1364/OE.22.026212; pmid: 25401653
75. A. Arbabi, Y. Horie, M. Bagheri, A. Faraon, Dielectric metasurfaces for complete control of phase and polarization with subwavelength spatial resolution and high transmission. *Nat. Nanotechnol.* **10**, 937–943 (2015). doi: 10.1038/nnano.2015.186; pmid: 26322944
76. S. Kruk *et al*., Broadband highly efficient dielectric metadevices for polarization control. *APL Photonics* **1**, 030801 (2016). doi: 10.1063/1.4949007
77. Z. Bomzon, V. Kleiner, E. Hasman, Pancharatnam-Berry phase in space-variant polarization-state manipulations with subwavelength gratings. *Opt. Lett.* **26**, 1424–1426 (2001). doi: 10.1364/OL.26.001424; pmid: 18049626
78. U. Levy, C.-H. Tsai, H.-C. Kim, Y. Fainman, Design, fabrication and characterization of subwavelength computer-generated holograms for spot array generation. *Opt. Express* **12**, 5345–5355 (2004). doi: 10.1364/OPEX.12.005345; pmid: 19484095
79. D. Lin, P. Fan, E. Hasman, M. L. Brongersma, Dielectric gradient metasurface optical elements. *Science* **345**, 298–302 (2014). doi: 10.1126/science.1253213; pmid: 25035488
80. M. Khorasaninejad *et al*., Metalenses at visible wavelengths: Diffraction-limited focusing and subwavelength resolution imaging. *Science* **352**, 1190–1194 (2016). doi: 10.1126/science.aaf6644; pmid: 27257251
81. Y. Yang *et al*., Dielectric meta-reflectarray for broadband linear polarization conversion and optical vortex generation. *Nano Lett.* **14**, 1394–1399 (2014). doi: 10.1021/nl4044482; pmid: 24547692
82. M. Decker *et al*., High-efficiency dielectric Huygens' surfaces. *Adv. Opt. Mater.* **3**, 813–820 (2015). doi: 10.1002/adom.201400584
83. C. Pfeiffer *et al*., Efficient light bending with isotropic metamaterial Huygens' surfaces. *Nano Lett.* **14**, 2491–2497 (2014). doi: 10.1021/nl5001746; pmid: 24689341
84. Y. F. Yu *et al*., High-transmission dielectric metasurface with 2π phase control at visible wavelengths. *Laser Photonics Rev.* **9**, 412–418 (2015). doi: 10.1002/lpor.201500041
85. K. E. Chong *et al*., Polarization-independent silicon metadevices for efficient optical wavefront control. *Nano Lett.* **15**, 5369–5374 (2015). doi: 10.1021/acs.nanolett.5b01752; pmid: 26192100
86. M. I. Shalaev *et al*., High-efficiency all-dielectric metasurfaces for ultracompact beam manipulation in transmission mode. *Nano Lett.* **15**, 6261–6266 (2015). doi: 10.1021/acs.nanolett.5b02926; pmid: 26280735
87. J. Du, Z. Lin, S. T. Chui, G. Dong, W. Zhang, Nearly total omnidirectional reflection by a single layer of nanorods. *Phys. Rev. Lett.* **110**, 163902 (2013). doi: 10.1103/PhysRevLett.110.163902; pmid: 23679606
88. C. J. Chang-Hasnain, W. Yang, High-contrast gratings for integrated optoelectronics. *Adv. Opt. Photonics* **4**, 379–440 (2012). doi: 10.1364/AOP.4.000379
89. S. Liu *et al*., Optical magnetic mirrors without metals. *Optica* **1**, 250 (2014). doi: 10.1364/OPTICA.1.000250
90. R. Paniagua-Domínguez *et al*., Generalized Brewster effect in dielectric metasurfaces. *Nat. Commun.* **7**, 10362 (2016). doi: 10.1038/ncomms10362; pmid: 26783075
91. C. Wu *et al*., Spectrally selective chiral silicon metasurfaces based on infrared Fano resonances. *Nat. Commun.* **5**, 3892 (2014). doi: 10.1038/ncomms4892; pmid: 24861488
92. Y. Yang, I. I. Kravchenko, D. P. Briggs, J. Valentine, All-dielectric metasurface analogue of electromagnetically induced transparency. *Nat. Commun.* **5**, 5753 (2014). doi: 10.1038/ncomms6753; pmid: 25511508
93. F. Aieta, M. A. Kats, P. Genevet, F. Capasso, Multiwavelength achromatic metasurfaces by dispersive phase compensation. *Science* **347**, 1342–1345 (2015). doi: 10.1126/science.aaa2494; pmid: 25700175
94. J. Sautter *et al*., Active tuning of all-dielectric metasurfaces. *ACS Nano* **9**, 4308–4315 (2015). doi: 10.1021/acsnano.5b00723; pmid: 25748581
95. P. P. Iyer, N. A. Butakov, J. A. Schuller, Reconfigurable semiconductor phased-array metasurfaces. *ACS Photonics* **2**, 1077–1084 (2015). doi: 10.1021/acsphotonics.5b00132
96. S. Jahani, Z. Jacob, All-dielectric metamaterials. *Nat. Nanotechnol.* **11**, 23–36 (2016). doi: 10.1038/nnano.2015.304; pmid: 26740041
97. L. Cao *et al*., Engineering light absorption in semiconductor nanowire devices. *Nat. Mater.* **8**, 643–647 (2009). doi: 10.1038/nmat2477; pmid: 19578337
98. L. Cao, J.-S. Park, P. Fan, B. Clemens, M. L. Brongersma, Resonant germanium nanoantenna photodetectors. *Nano Lett.* **10**, 1229–1233 (2010). doi: 10.1021/nl9037278; pmid: 20230043
99. M. Garín *et al*., All-silicon spherical-Mie-resonator photodiode with spectral response in the infrared region. *Nat. Commun.* **5**, 3440 (2014). doi: 10.1038/ncomms4440; pmid: 24614644
100. G. Grzela *et al*., Nanowire antenna emission. *Nano Lett.* **12**, 5481–5486 (2012). doi: 10.1021/nl301907f; pmid: 23030698
101. J. A. Schuller, T. Taubner, M. L. Brongersma, Optical antenna thermal emitters. *Nat. Photonics* **3**, 658–661 (2009). doi: 10.1038/nphoton.2009.188
102. L. Cao *et al*., Semiconductor nanowire optical antenna solar absorbers. *Nano Lett.* **10**, 439–445 (2010). doi: 10.1021/nl9036627; pmid: 20078065
103. J. Grandidier, D. M. Callahan, J. N. Munday, H. A. Atwater, Light absorption enhancement in thin-film solar cells using whispering gallery modes in dielectric nanospheres. *Adv. Mater.* **23**, 1272–1276 (2011). doi: 10.1002/adma.201004393; pmid: 21381129
104. M. L. Brongersma, Y. Cui, S. Fan, Light management for photovoltaics using high-index nanostructures. *Nat. Mater.* **13**, 451–460 (2014). doi: 10.1038/nmat3921; pmid: 24751773
105. F. Priolo, T. Gregorkiewicz, M. Galli, T. F. Krauss, Silicon nanostructures for photonics and photovoltaics. *Nat. Nanotechnol.* **9**, 19–32 (2014). doi: 10.1038/nnano.2013.271; pmid: 24390564
106. S. J. Kim *et al*., Light trapping for solar fuel generation with Mie resonances. *Nano Lett.* **14**, 1446–1452 (2014). doi: 10.1021/nl404575e; pmid: 24524658
107. S. J. Kim, P. Fan, J.-H. Kang, M. L. Brongersma, Creating semiconductor metafilms with designer absorption spectra. *Nat. Commun.* **6**, 7591 (2015). doi: 10.1038/ncomms8591; pmid: 26184335

ACKNOWLEDGMENTS

We thank I. Brener, A. Krasnok, D. Neshev, I. Staude, and J. Valentine for useful discussions and R. Paniagua for help with design of the figures. Supported by the DSI core fund and A*STAR Science and Engineering Research Council Pharos grant 1527000025 (A.I.K. and B.L.); the Australian Research Council (A.E.M. and Y.S.K.); and U.S. Air Force Office of Scientific Research grant FA9550-14-1-0389 and the U.S. Department of Energy (DOE) Light-Material Interactions Energy Frontier Research Center, an Energy Frontier Research Center funded by the DOE Office of Science, Basic Energy Sciences, under award DE-SC0001293 (M.L.B.).

10.1126/science.aag2472

Downloaded from https://www.science.org at Moscow State University on March 10, 2022

Science

Optically resonant dielectric nanostructures

Arseniy I. KuznetsovAndrey E. MiroshnichenkoMark L. BrongersmaYuri S. KivsharBoris Luk'yanchuk

Science, 354 (6314), aag2472. • DOI: 10.1126/science.aag2472

A clear approach to nanophotonics

The resonant modes of plasmonic nanoparticle structures made of gold or silver endow them with an ability to manipulate light at the nanoscale. However, owing to the high light losses caused by metals at optical wavelengths, only a small fraction of plasmonics applications have been realized. Kuznetsov *et al.* review how high-index dielectric nanoparticles can offer a substitute for these metals, providing a highly flexible and low-loss route to the manipulation of light at the nanoscale.

Science, this issue p. 10.1126/science.aag2472

View the article online
https://www.science.org/doi/10.1126/science.aag2472
Permissions
https://www.science.org/help/reprints-and-permissions

Use of this article is subject to the Terms of service

Science (ISSN 1095-9203) is published by the American Association for the Advancement of Science. 1200 New York Avenue NW, Washington, DC 20005. The title *Science* is a registered trademark of AAAS.
Copyright © 2016, American Association for the Advancement of Science

Downloaded from https://www.science.org at Moscow State University on March 10, 2022